INTERNATIONAL JOURNAL FOR NUMERICAL METHODS IN ENGINEERING
Int. J. Numer. Meth. Engng 2003; **56**:117–144 (DOI: 10.1002/nme.559)

New approaches for error estimation and adaptivity for 2D potential boundary element methods

Ariosto B. Jorge[1,2,*,†], Gabriel O. Ribeiro[3] and Timothy S. Fisher[2]

[1]*Department of Mathematics and Computer Sciences, UNIFEI – Federal University at Itajubá, Av BPS, 1303, Itajubá, MG, CEP 37500-000, Brazil*
[2]*Department of Mechanical Engineering, Vanderbilt University, Nashville, TN 37235, U.S.A.*
[3]*Department of Structural Engineering, UFMG – Federal University of Minas Gerais, Av do Contorno, 842 - 2o andar, Belo Horizonte, MG, CEP 30110-060, Brazil*

SUMMARY

This work presents two new error estimation approaches for the BEM applied to 2D potential problems. The first approach involves a local error estimator based on a gradient recovery procedure in which the error function is generated from differences between smoothed and non-smoothed rates of change of boundary variables in the local tangential direction. The second approach involves the external problem formulation and gives both local and global measures of error, depending on a choice of the external evaluation point. These approaches are post-processing procedures. Both estimators show consistency with mesh refinement and give similar qualitative results. The error estimator using the gradient recovery approach is more general, as this formulation does not rely on an 'optimal' choice of an external parameter. This work presents also the use of a local error estimator in an adaptive mesh refinement procedure. This *r*-refinement approach is based on the minimization of the standard deviation of the local error estimate. A non-linear programming procedure using a feasible-point method is employed using Lagrange multipliers and a set of active constraints. The optimization procedure produces finer meshes close to a singularity and results that are consistent with the problem physics. Copyright © 2002 John Wiley & Sons, Ltd.

KEY WORDS: boundary element methods (BEM); error estimators; gradient recovery; adaptivity; nonlinear programming; optimization; feasible-point method; Lagrange multipliers

1. INTRODUCTION

Boundary integral equation (BIE) formulations are exact representations of boundary value problems (BVPs). Errors may appear in the discretization process leading to the boundary

*Correspondence to: Ariosto B. Jorge, Department of Mathematics and Computer Science, UNIFEI – Federal University at Itajubá, Av BPS, 1303, Itajubá, MG, CEP 37500-000, Brazil
†E-mail: ariosto.b.jorge@unifei.edu.br

Contract/grant sponsor: CNPq—Conselho Nacional de Desenvolvimento Científico e Tecnológico
Contract/grant sponsor: FAPEMIG—Fundação de Amparo à Pesquisa do Estado de Minas Gerais
Contract/grant sponsor: National Science Foundation; contract/grant number: CTS-9983961

Received 5 September 2001
Revised 5 November 2001
Accepted 6 March 2002

element method (BEM) because the BIE is valid only at a finite number of collocation points. Local and global contributions to these errors can be estimated and used in mesh refinement. Error estimators based on residuals and error norms, similar to the approaches available in the finite element method (FEM), have been used for symmetric BEM formulations, but the error estimators literature is scarce for collocation BEM formulations [1]. In the present work, two local error estimation approaches are presented for 2D potential problems. These approaches can be used for both Galerkin and collocation BEM formulations and can be extended to potential and elastostatics problems in 2D or 3D. This work presents also an adaptive mesh refinement procedure that can be used in conjunction with any local error estimator to equalize the distribution of the local error through the various elements. This *r*-refinement procedure can be used to resize elements before an *h*- or *p*-refinement is performed, thereby making mesh refinement more efficient.

To solve the BIE numerically, the boundary is divided into elements. The collocation BEM is a discretization of a BIE so that the solution is only valid at a finite number of boundary collocation points. For the other boundary points, interpolating functions approximate dependent variables of the problem. Several sources of error exist in this approach. First, the discretized boundary may not represent the original one. Second, polynomial interpolation is only an approximation of the variable within the element. Third, the continuity of the boundary elements may not satisfy the smoothness requirements of the original BIE. Fourth, numerical integration using Gaussian quadrature is an approximation of the integral being evaluated. Local and global contributions to the error due to an element can be estimated so that mesh refinement can be performed to minimize these errors. A global error estimator can be used to determine the need for refinement, while a local error estimator can be used to determine which portions of the boundary require refinement in an adaptive process.

Several types of *a posteriori* error estimators for BEM have been proposed in the literature, primarily for symmetric BEM, and only a few have been studied for collocation BEM. Reviews for error estimation and adaptivity methods can be found in Liapis [1] and Kita and Kamiya [2, 3]. These error estimators include various versions of element residual methods, flux projection estimators, extrapolation error estimators and estimators measuring the sensitivity of the numerical solution to a shift in the collocation point. Kelly *et al.* [4] proposed a global error estimator based on the energy norm. Carstensen and co-workers presented *a posteriori* error estimates [5] and adaptive procedures [6, 7] based on symmetric Galerkin BEM formulations, for which upper and lower bounds of the error can be computed. A measure of the efficiency for the Galerkin formulation was also established [8]. Liang *et al.* [9] proposed local error estimators based on dual BIE formulations. Paulino *et al.* [10] and Menon *et al.* [11] proposed a *pointwise* error estimator based on the difference between two formulations, the standard formulation and the hypersingular formulation. This approach was applied to a symmetric-Galerkin BEM formulation by Paulino and Gray [12]. Denda and Dong [13] proposed an error estimator for the direct collocation method in the elastostatics problem. In this case, a comparison with an equivalent representation of the same problem, obtained for the exterior domain, is performed. Jou and Liu [14] obtained upper and lower bounds for error using a residual approach. Sensitivities to variations in node location are found in References [15–18]. Varfolomeyev *et al.* [19] employed an averaged error estimation technique. Zhan and Yokoyama [20] obtained the element degree from a normalized integral of the squared error. Karafiat [21] presented an *a priori* convergence estimate, requiring a special procedure for singular and nearly singular integrals. Liapis [22] presented a residual error estimator. Error

estimators based on differences between the BEM solution and the element approximation or interpolation can be found in Chao and Lee [23] and in Zhao [24]. Ammons and Vable [25] employed a L_1 norm as a measure of error.

Most the above cited error estimators in BEM fall into three categories: average in the norm, sensitivity analysis and difference between two equivalent formulations. An error estimator based in the difference between two equivalent formulations is developed in the present work. Gradient recovery, when properly adapted from the FEM formulations, is a fourth promising category and is developed in the present work.

Two *a posteriori* error estimator approaches for the collocation BEM are considered in detail in Section 2 for 2D potential problems. The first approach is a local error estimator based on a gradient recovery procedure, wherein the smoothed or recovered functions are rates of change of the boundary variables in the local tangential direction. The gradient recovery approach is commonly used in the finite element method [26–28] and considers the evaluation of the gradient of the field variable in global co-ordinates, allowing for continuous derivatives of this field variable in fixed global directions. On the other hand, in the BEM the variables of interest are written in local co-ordinates, so that the flux is the boundary variable associated with the outward local normal derivative of the potential. The potential is continuous throughout the boundary, while the flux and the tangential derivative of the potential may be discontinuous, such as where the boundary is not smooth. Any recovery procedure of the tangential derivatives must allow for these inter-element discontinuities.

The second error estimator approach is associated with an external problem formulation and gives both a local and a global measure of the error, depending on the location of the external point where the equation is applied. The potential should vanish at points in the exterior of the domain due to the fact that the swept angle appearing in the boundary integral formulation is zero. Non-zero values indicate errors. By collocating the external point near the boundary, the influence of nearby elements on the error estimate will be dominant, so that the error information can be considered to be local.

These two error estimation approaches represent a post-processing step, after a BEM solution is known. The exact solution is not required for either error estimator. In the present work, the two estimates are computed for two 2D potential problems, one containing a singularity and the other with a known exact solution, and a comparison is made between both estimators. The error consistency with mesh refinement is also compared for both error estimators.

An approach to use a local error estimator in an adaptive mesh refinement procedure is presented in Section 4. Sun and Zamani [29] presented an adaptive $h-r$ refinement algorithm for the Laplace equation based the minimization of an upper bound of a residual to obtain an asymptotically optimal grading function. This approach was highly dependent on the weakness of the singularities involved in the Laplacian operator and on the existence of a grading function. Zamani and Sun [30] discussed also the implementation of r and $h-r$ refinement-redistribution techniques. In Kita *et al.* [31] a relationship between error and element size is established, and the goal is to redistribute the error on the elements. One step in the algorithm is to discretize (re-mesh) macro-elements in order to redistribute the error. Apparently this step in Reference [31] is not automated, and requires external intervention and decision-making on nodal repositioning.

The adaptive r-refinement procedure presented in this work is based on a constrained optimization algorithm. An r-refined mesh is automatically obtained as a result of the

procedure. Also, the proposed mesh refinement approach employs an optimization procedure that is not limited to the collocation BEM and could be used for the refinement of any BEM formulation. This procedure is not limited by the weakness of the singularities in the BEM formulation. After a local error estimator is chosen, it can be used for mesh refinement. The adaptive mesh refinement procedure is independent of the choice of the local error estimator and is based on the minimization of the standard deviation of the normalized local error estimate.

The local error estimator for the BEM is a function of nodal positions, which can be modified within certain limits, producing inequality constraints for these positions. Local error estimates are evaluated for several different meshes to provide a quadratic interpolation of the objective function. Design of experiments techniques are adapted to this problem to generate this second-order model. A non-linear programming procedure using a feasible-point method is employed, based on the use of Lagrange multipliers and a set of active constraints. The optimization procedure produces finer meshes near the singularity point. This result is consistent with the problem physics, as the accuracy of the BEM solution is expected to increase when greater element density exists near the singular point.

2. PROPOSED *A POSTERIORI* ERROR ESTIMATORS FOR BEM

Two error estimators for BEM are considered in detail in the present work. The first is based on the gradient recovery approach, and the second is based on the error with respect to an external formulation. These error estimators require only post-processing procedures that generate qualitative indicators of the local errors of the discretized BEM solution for a specified boundary mesh. They are suitable to be used for the collocation BEM, for which other error estimators (such as those that require energy norms) may not be available.

2.1. The gradient recovery approach for error estimation in BEM

The following discussion is limited to 2D potential theory, but the ideas can be adapted to 3D problems and to elasticity theory. The concept of recovery of derivatives for error estimation originated with finite element methods, in which error indicators were derived from derivatives of the computed finite element solution. Even small errors in the finite element solution could lead to large errors or inaccuracy in these derivatives. Smoothed or refined approximations for the derivatives were developed so that the error indicators depending on these derivatives would be more credible. A procedure to smooth the gradient to compute these derivatives with good accuracy is called gradient recovery [26–28]. The derivatives are evaluated from a weighted average of element derivatives surrounding a node. The weighting factors are the element areas. The FEM procedure is illustrated below for a one-dimensional problem for simplicity. For each element (e), the first derivatives are expressed in terms of the derivatives of the shape functions N and of the nodal values of the potential solution $\{\phi\}^{(e)}$ as

$$\left(\frac{\partial \phi}{\partial x}\right)^{(e)} = \left[\frac{\partial N}{\partial x}\right] \{\phi\}^{(e)} \tag{1}$$

These first derivatives can be written in an average sense as

$$\left(\frac{\partial \phi}{\partial x}\right)^{(e)*} = \lfloor N \rfloor \left\{\frac{\partial \phi}{\partial x}\right\}^{(e)*} \tag{2}$$

where the goal is to find the vector of smoothed (or 'recovered') nodal derivatives of the potential $\{\partial\phi/\partial x\}^{(e)*}$. An equivalence equation can now be written in a region $\Omega^{(e)}$ surrounding an element (e) as

$$\int_{\Omega^{(e)}} \{N\} \left(\frac{\partial \phi}{\partial x}\right)^{(e)*} \mathrm{d}A = \int_{\Omega^{(e)}} \{N\} \left(\frac{\partial \phi}{\partial x}\right)^{e} \mathrm{d}A$$

$$\Rightarrow \int_{\Omega^{(e)}} \{N\} \lfloor N \rfloor \, \mathrm{d}A \left\{\frac{\partial \phi}{\partial x}\right\}^{(e)*} = \int_{\Omega^{(e)}} \{N\} \left\lfloor \frac{\partial N}{\partial x} \right\rfloor \mathrm{d}A \{\phi\}^{(e)} \tag{3}$$

The element equations in Equation (3) are then assembled for the entire domain Ω. The vector of smoothed nodal derivatives $\{\partial\phi/\partial x\}^{(e)*}$ can be obtained from the assembled system of equations. An important feature in this procedure is that the x-co-ordinate belongs to a global co-ordinate system, so that not only is the potential field at the nodes $\{\phi\}^{(e)}$ continuous in Ω, but also all the elements of the smoothed gradient vector $\{\partial\phi/\partial x\}^{(e)*}$ in a general problem are continuous in Ω when linear or higher order elements are used. The difference between this refined gradient and the actual gradient for a certain mesh provides an error measure.

This post-processing approach to find error estimators from gradient recovery can be adapted to BEM problems after the solution is known for all nodes on the boundary. Consider first an element (e) of the boundary region in which the gradient is being evaluated. Let ϕ be the potential, $\partial\phi/\partial s$ be the tangential derivative of ϕ, and $q = \partial\phi/\partial n$ be the flux. From the BEM solution, the nodal values $\phi_i^{(e)}$ and $q_i^{(e)}$ are known. Both the flux q and the tangential derivative $\partial\phi/\partial s$ are allowed to be discontinuous at boundary points where the normal unit vector is not unique. For C^0 elements, the tangential and normal unit vectors are uniquely defined only locally in the interior of a boundary element. The usual BEM solution allows for these discontinuities to occur, and the flux solution on the boundary is given both as a function of the node number i and of the element number (e). Thus, on a certain node i, the flux on the element before the node $q_i^{(e)}$ might be different from the flux for the element after the node $q_i^{(e+1)}$. The same discontinuities will apply for both the original and the recovered or smoothed values of the tangential derivative of the potential $\partial\phi/\partial s$ at the same boundary nodes where the flux is discontinuous.

To write a system of equations similar to the one obtained with the FEM procedure, continuity would be required for the derivatives of the potential. But the derivatives of the potential are continuous only in a global co-ordinate system. These derivatives are not continuous in local co-ordinate systems along the boundary curve if the boundary has corners. The approach adopted in this work is to introduce double nodes at all the discontinuity points, such as the corner nodes on the boundary. Elements with zero length connect these double nodes, so that no local or global contribution for the error from these ficticious elements is incurred. It must be noted that the gradient recovery approach is a post-processing procedure that is completely independent of the BEM formulation that was used to obtain the boundary solution, which may or may not use originally a double-node approach. The concept of double nodes to

account for the flux discontinuities when obtaining the boundary solution is well known in the BEM literature [32] but is not used in this work. The double nodes introduced here originate from discontinuities in the values of q and $\partial\phi/\partial s$ at corner nodes in the post-processing algorithm to obtain the element errors and not from the original BEM procedure to evaluate the boundary solution.

The solution at any point inside the element is $\phi^{(e)}(\xi) = \lfloor N \rfloor \{\phi\}^{(e)} = \sum_{i=1}^{m} N_i(\xi)\phi_i^{(e)}$ and $q^{(e)}(\xi) = \lfloor N \rfloor \{q\}^{(e)} = \sum_{i=1}^{m} N_i(\xi) q_i^{(e)}$, where ξ is the intrinsic co-ordinate and m is the number of element nodes corresponding to the polynomial interpolation being used, such as $m = 2$ for linear elements, $m = 3$ for quadratic elements, etc. Taking derivatives with respect to the intrinsic co-ordinate gives

$$\left(\frac{\mathrm{d}\phi}{\mathrm{d}s}\right)^{(e)} = \left(\frac{\mathrm{d}\phi}{\mathrm{d}\xi}\right)^{(e)} \left(\frac{\mathrm{d}\xi}{\mathrm{d}s}\right)^{(e)}, \quad \left(\frac{\mathrm{d}q}{\mathrm{d}s}\right)^{(e)} = \left(\frac{\mathrm{d}q}{\mathrm{d}\xi}\right)^{(e)} \left(\frac{\mathrm{d}\xi}{\mathrm{d}s}\right)^{(e)} \tag{4}$$

where

$$\left(\frac{\mathrm{d}\phi}{\mathrm{d}\xi}\right)^{(e)} = \left\lfloor \frac{\mathrm{d}N}{\mathrm{d}\xi} \right\rfloor \{\phi\}^{(e)}, \quad \left(\frac{\mathrm{d}q}{\mathrm{d}\xi}\right)^{(e)} = \left\lfloor \frac{\mathrm{d}N}{\mathrm{d}\xi} \right\rfloor \{q\}^{(e)}$$

and $(\mathrm{d}\xi/\mathrm{d}s)^{(e)} = J(\xi, s)$ is the Jacobian of the transformation between the real element (with co-ordinate s) and the standard element (with the intrinsic co-ordinate ξ).

These derivatives can be written with polynomial shape functions one degree higher as

$$\left(\frac{\mathrm{d}\phi}{\mathrm{d}s}\right)^{(e)*} = \lfloor N \rfloor \left\{\frac{\mathrm{d}\phi}{\mathrm{d}s}\right\}^{(e)*}, \quad \left(\frac{\mathrm{d}q}{\mathrm{d}s}\right)^{(e)*} = \lfloor N \rfloor \left\{\frac{\mathrm{d}q}{\mathrm{d}s}\right\}^{(e)*} \tag{5}$$

where $\{\mathrm{d}\phi/\mathrm{d}s\}^{(e)*}$ and $\{\mathrm{d}q/\mathrm{d}s\}^{(e)*}$ are the sets of nodal values of the corresponding derivatives that are equivalent in a local averaging sense to the original ones, $\{\mathrm{d}\phi/\mathrm{d}s\}^{(e)}$ and $\{\mathrm{d}q/\mathrm{d}s\}^{(e)}$. Element equivalence is enforced by requiring that both formulations for the derivatives give same element integrals, defined by

$$\begin{aligned} I_{\phi}^{(e)} &= \int_{S^{(e)}} \{N\} \left(\frac{\mathrm{d}\phi}{\mathrm{d}s}\right)^{(e)*}, \quad \mathrm{d}s = \int_{S^{(e)}} \{N\} \left(\frac{\mathrm{d}\phi}{\mathrm{d}\xi}\right)^{(e)} J(\xi, s)\,\mathrm{d}s \\ I_{q}^{(e)} &= \int_{S^{(e)}} \{N\} \left(\frac{\mathrm{d}q}{\mathrm{d}s}\right)^{(e)*}, \quad \mathrm{d}s = \int_{S^{(e)}} \{N\} \left(\frac{\mathrm{d}q}{\mathrm{d}\xi}\right)^{(e)} J(\xi, s)\,\mathrm{d}s \end{aligned} \tag{6}$$

where the integration is performed on $S^{(e)}$, which is the element length in 2D or the element area in 3D. If the element under integration is now written as $\mathrm{d}s = J(s, \xi)\,\mathrm{d}\xi$, where $J(s, \xi) = \mathrm{d}s/\mathrm{d}\xi = 1/J(\xi, s)$, all terms in the integrands are now only functions of the intrinsic variable ξ, and all element integrations are now performed for $\xi \in [-1, 1]$, for the usual Lagrangian interpolating functions.

The element equations in Equation (6) are then assembled for the entire boundary S, leading to an expanded system of equations that includes the original elements and the new zero-length elements at the double nodes. A simple procedure is implemented in this work to account automatically for these new zero-length elements when assembling the system of equations. In the first step, a new variable $\mathrm{LC}(i)$ is created as a corner locator and set initially as $\mathrm{LC}(i) = 0$

for all nodes $i = 1, \ldots, N$. Then a test is performed at each node i, for discontinuities in the normal unit vector between the elements that share the node. If the normal unit vector in both elements that share the node is not unique, a corner is located, and $\mathrm{LC}(i) = 1$. If the boundary surface is smooth at this node, the procedure then evaluates the flux to check for discontinuities between elements. If the flux is discontinuous at a node on a smooth part of the boundary, this node is also treated as a 'corner' that needs a double node to be added, and $\mathrm{LC}(i)$ is set to one.

The second step is to renumber the current nodes and elements to include the zero-length elements at the located 'corner' nodes. For every node i where a 'corner' exists, a new node/element is created with corresponding number $i + 1$, and all subsequent nodes and elements have their numbers increased by one. The value of the potential at node i is assigned to both nodes of the zero-length element. The flux at node i in the element before the node is assigned to the first node of the zero-length element, and the flux in the element after node i is assigned to the second node of the zero-length element. A new augmented connectivity matrix is thus created relating node/element numbering, including the added zero-length elements. With this procedure, single values for the flux and for the tangential derivatives of both the potential and the flux can be assigned to each node in the augmented system.

By assembling the element equations, an augmented system of equations is thus obtained from which the vectors of smoothed nodal derivatives $\{\partial\phi/\partial s\}^{(e)*}$ and $\{\partial q/\partial s\}^{(e)*}$ can be obtained. The system matrix for the coefficients of the recovered or smoothed quantities is not singular and admits an inverse after assembling all elements, including the zero-length elements that link the double nodes. The third step is to evaluate the element errors still in the augmented system and then renumber backwards the nodes/elements down to their original numbering, by excluding the zero-length elements so that only the error information of the original elements remains.

The gradient recovery procedure is based on an algorithm that includes all the boundary elements. Thus, the smoothed tangential derivatives of the densities (the potential and the flux) are not obtained independently for each element. Instead, a unique value for the smoothed or recovered nodal values of the tangential derivatives of the densities is only obtained when all the element matrices are assembled.

Several approaches could be employed to use the assembly of the element integrals obtained in Equation (6). By assembling the element integrals of the type $I_{\phi}^{(e)}$ only, an expression for the local error related to the tangential derivative of ϕ could be obtained. Similarly, by assembling the integrals of the type $I_{q}^{(e)}$ only, an expression for the local error related to the tangential derivative of the flux q could be obtained. A more elaborate expression for the error related to both the tangential and the normal derivatives of the potential could be obtained by combining both integrals.

The above three approaches are implemented in this work so that error estimators are obtained separately from the smoothed tangential derivatives of the potential and of the flux, and also a combined error estimator is obtained when the individual contributions from the potential and flux tangential derivatives are added. A parameter is introduced so that the individual contributions are scaled before being added. In all cases, only the tangential derivatives of the densities are smoothed.

When considering the gradient of the potential written in terms of its tangential and normal components, the tangential derivative of the potential, being written with a polynomial with one degree less than the flux, appears to be the component of the gradient that gives the most

significant contribution for the total element error. Jorge *et al.* [35] shows that accurate results for the potential and the flux were obtained for coarse graded meshes where the tangential derivatives of the potential were better approximated. In the following, the error estimators are implemented for linear elements by using only the recovery of the tangential derivatives of the densities.

With this approach, the degree of the interpolating polynomial for the recovered tangential derivative increases by one, while the degree of the normal derivative stays the same. A measure of the error is the difference between the refined and the actual tangential derivatives. This approach is well adapted to obtain element error information in the boundary parts where the tangential derivative varies rapidly, and its polynomial representation is inaccurate. This procedure could be easily extended for higher order elements.

2.1.1. Implementation of the tangential derivative recovery for linear elements. The recovery of the tangential derivative of the potential is now detailed to obtain an error estimator for a BEM code implemented with linear elements. A standard linear element has two end nodes with corresponding shape functions $N_1(\xi)=(1-\xi)/2$ and $N_2(\xi)=(1+\xi)/2$ for $\xi\in[-1,1]$. The shape function derivatives are $N_1'(\xi)=-1/2$ and $N_2'(\xi)=1/2$. The Jacobian for this 1D straight element is $J(\xi,s)=\partial\xi/\partial s=2/L^{(e)}$, where $L^{(e)}$ is the length of the boundary element (e), so the element of integration is $dS^{(e)}=(L^{(e)}/2)\,\mathrm{d}\xi$. The original (non-smoothed) and the recovered (smoothed, denoted by $*$) tangential derivatives of the potential are written for the element (e) as

$$\left(\frac{\partial\phi}{\partial s}\right)^{(e)}(\xi)=\left\lfloor\frac{\partial N}{\partial s}\right\rfloor\{\phi\}^{(e)}=\left\lfloor\frac{\partial N}{\partial\xi}\right\rfloor\frac{\partial\xi}{\partial s}\{\phi\}^{(e)}=\frac{2}{L^{(e)}}\lfloor N_1'(\xi)\;\;N_2'(\xi)\rfloor\begin{Bmatrix}\phi_1^{(e)}\\ \phi_2^{(e)}\end{Bmatrix}\tag{7}$$

$$\left(\frac{\partial\phi}{\partial s}\right)^{(e)*}(\xi)=\lfloor N_1(\xi)\;\;N_2(\xi)\rfloor\begin{Bmatrix}\dfrac{\partial\phi_1^{(e)*}}{\partial s}\\ \dfrac{\partial\phi_2^{(e)*}}{\partial s}\end{Bmatrix}\tag{8}$$

so that the equivalence in the element can be enforced. Starting from the first equation in Equation (6), the various steps to obtain the element integrals are detailed as follows:

$$\int_{S^{(e)}}\{N\}\lfloor N\rfloor\,\mathrm{d}s^{(e)}\begin{Bmatrix}\dfrac{\partial\phi^{(e)*}}{\partial s}\end{Bmatrix}=\int_{S^{(e)}}\{N\}\,\mathrm{d}s^{(e)}\frac{\partial\phi^{(e)}}{\partial s}$$

$$\int_{-1}^{1}\begin{Bmatrix}N_1(\xi)\\ N_2(\xi)\end{Bmatrix}\lfloor N_1(\xi)\;\;N_2(\xi)\rfloor\frac{L^{(e)}}{2}\,\mathrm{d}\xi\begin{Bmatrix}\dfrac{\partial\phi_1^{(e)*}}{\partial s}\\ \dfrac{\partial\phi_2^{(e)*}}{\partial s}\end{Bmatrix}=\int_{-1}^{1}\begin{Bmatrix}N_1(\xi)\\ N_2(\xi)\end{Bmatrix}\frac{L^{(e)}}{2}\,\mathrm{d}\xi\frac{2}{L^{(e)}}$$

$$\times\lfloor N_1'(\xi)\;\;N_2'(\xi)\rfloor\begin{Bmatrix}\phi_1^{(e)}\\ \phi_2^{(e)}\end{Bmatrix}$$

$$\frac{L^{(e)}}{2}\begin{bmatrix}\int_{-1}^{1} N_1N_1\,\mathrm{d}\xi & \int_{-1}^{1} N_1N_2\,\mathrm{d}\xi\\ \int_{-1}^{1} N_2N_1\,\mathrm{d}\xi & \int_{-1}^{1} N_2N_2\,\mathrm{d}\xi\end{bmatrix}\begin{Bmatrix}\dfrac{\partial\phi_1^{(e)*}}{\partial s}\\ \dfrac{\partial\phi_2^{(e)*}}{\partial s}\end{Bmatrix}=\begin{bmatrix}\int_{-1}^{1} N_1N_1'\,\mathrm{d}\xi & \int_{-1}^{1} N_1N_2'\,\mathrm{d}\xi\\ \int_{-1}^{1} N_2N_1'\,\mathrm{d}\xi & \int_{-1}^{1} N_2N_2'\,\mathrm{d}\xi\end{bmatrix}\begin{Bmatrix}\phi_1^{(e)}\\ \phi_2^{(e)}\end{Bmatrix}$$

After substituting the shape functions and performing the integrals, the element equivalence equation is obtained in matrix form as

$$\frac{L^{(e)}}{3}\begin{bmatrix}2 & 1\\ 1 & 2\end{bmatrix}\begin{Bmatrix}\dfrac{\partial\phi_1^{(e)*}}{\partial s}\\ \dfrac{\partial\phi_2^{(e)*}}{\partial s}\end{Bmatrix}=\begin{bmatrix}-1 & 1\\ -1 & 1\end{bmatrix}\begin{Bmatrix}\phi_1^{(e)}\\ \phi_2^{(e)}\end{Bmatrix} \tag{9}$$

Now all element matrices given by Equation (9) can be assembled for a particular mesh with N elements. By solving the assembled system of equations, the vector of nodal values for the smoothed tangential derivatives of the potential $\{\partial\phi/\partial s\}^{(e)*}$ is obtained. Because the assembled matrices are sparse, special methods can be used to solve the assembled system [33]. The vector of element interpolations for the original non-zero elements (e) is now obtained from the first equation in Equation (5) as

$$\left(\frac{\partial\phi}{\partial s}(\xi)\right)^{(e)*}=N_1(\xi)\frac{\partial\phi_1^{(e)*}}{\partial s}+N_2(\xi)\frac{\partial\phi_2^{(e)*}}{\partial s} \tag{10}$$

The residuals $r^2_{\phi^{(e)}}$ are now evaluated for each of these elements as the square of the differences between the smoothed solution obtained in Equation (10) and the original non-smoothed solution obtained from the first equation in Equation (4).

$$r^2_{\phi^{(e)}}(\xi)=\left[\left(\frac{\partial\phi}{\partial s}(\xi)\right)^{(e)*}-\frac{2}{L^{(e)}}\lfloor N_1'(\xi)\ N_2'(\xi)\rfloor\begin{Bmatrix}\phi_1\\ \phi_2\end{Bmatrix}^{(e)}\right]^2 \tag{11}$$

The element errors $E_{\phi^{(e)}}$, the average error $E_{\phi_{\mathrm{AVE}}}$ and the normalized element errors $E_{\phi^{(e)}_{\mathrm{norm}}}$ are

$$E_{\phi^{(e)}}=\left[\int_{-1}^{1} r^2_{\phi^{(e)}}(\xi)\,\mathrm{d}\xi\right]^{1/2}\frac{L^{(e)}}{L_{\mathrm{total}}}\quad E_{\phi_{\mathrm{AVE}}}=\frac{1}{N}\sum_{(e)}E_{\phi^{(e)}}\quad E_{\phi^{(e)}_{\mathrm{norm}}}=\frac{E_{\phi^{(e)}}}{E_{\phi_{\mathrm{AVE}}}} \tag{12}$$

where L_{total} is the length of the entire boundary. The element errors $E_{\phi^{(e)}}$ are obtained as the square root of the integral of the element residuals, weighted by the relative element length to account for element sizes while evaluating the average error $E_{\phi_{\mathrm{AVE}}}$. The average error is a measure of the global error and is used to obtain the normalized element errors $E_{\phi^{(e)}_{\mathrm{norm}}}$ so

that this normalized local error indicator can be used in an adaptive procedure. If $E_{\phi^{(e)}_{\text{norm}}} \gg 1$, then the local error in the element is much larger than the average, and a mesh refinement is needed. This refinement could be achieved either by reducing the size of the elements in this boundary region (h-refinement) or by increasing the order of the polynomial interpolant in the element (p-refinement). If $E_{\phi^{(e)}_{\text{norm}}} \cong 1$ or $E_{\phi^{(e)}_{\text{norm}}} < 1$, the local error has an average or better value, and no refinement is needed. A similar procedure on flux components, by replacing ϕ by q in the above equations, generates smoothed tangential derivatives of the flux, element residuals $r^2_{q^{(e)}}(\xi)$, element errors $E_{q^{(e)}}$, average error $E_{q_{\text{AVE}}}$ and normalized element errors $E_{q^{(e)}_{\text{norm}}}$.

A more general local error estimator is obtained when combining the contributions for the element error as evaluated from the recovery of the tangential derivatives of both the potential and the flux. The non-normalized element errors are combined by addition after scaling. In this work, scaling factors for the tangential derivatives of both the potential and the flux were constructed by evaluating average values of these tangential derivatives in each finite length element and adding these element contributions to the scaling factor after weighting the element contribution by the relative element length. Each element contribution for the scaling factor is an average of the element tangential derivative of the density, as evaluated using the smoothed and the non-smoothed variables. The element contribution for the scaling factor for the tangential derivative of the potential is obtained as follows:

$$\text{SF}_{\phi^{(e)}} = \frac{[(\mathrm{d}\phi/\mathrm{d}s)^{(e)*}_{\text{AVE}}]^2 + [(\mathrm{d}\phi/\mathrm{d}s)^{(e)}_{\text{AVE}}]^2}{2} \frac{L^{(e)}}{L_{\text{total}}} \tag{13}$$

where the element average using smoothed variables is given by

$$\left(\frac{\mathrm{d}\phi}{\mathrm{d}s}\right)^{(e)*}_{\text{AVE}} = \frac{1}{L^{(e)}} \int_{S^{(e)}} \frac{\mathrm{d}\phi}{\mathrm{d}s}^{(e)*} \mathrm{d}s = \frac{1}{2} \int_{-1}^{1} \lfloor N_1(\xi)\ N_2(\xi) \rfloor \, \mathrm{d}\xi \begin{Bmatrix} \dfrac{\mathrm{d}\phi_1}{\mathrm{d}s}^{(e)*} \\ \dfrac{\mathrm{d}\phi_2}{\mathrm{d}s}^{(e)*} \end{Bmatrix}$$

$$\Rightarrow \left(\frac{\mathrm{d}\phi}{\mathrm{d}s}\right)^{(e)*}_{\text{AVE}} = \begin{bmatrix} \frac{1}{2} & \frac{1}{2} \end{bmatrix} \begin{Bmatrix} \dfrac{\mathrm{d}\phi_1}{\mathrm{d}s}^{(e)*} \\ \dfrac{\mathrm{d}\phi_2}{\mathrm{d}s}^{(e)*} \end{Bmatrix} \tag{14}$$

and the element average using non-smoothed variables is given by

$$\left(\frac{\mathrm{d}\phi}{\mathrm{d}s}\right)^{(e)}_{\text{AVE}} = \frac{1}{L^{(e)}} \int_{S^{(e)}} \frac{\mathrm{d}\phi}{\mathrm{d}s}^{(e)} \mathrm{d}s = \frac{1}{2} \int_{-1}^{1} \lfloor N_1'(\xi)\ N_2'(\xi) \rfloor \frac{2}{L^{(e)}} \, \mathrm{d}\xi \begin{Bmatrix} \phi_1^{(e)} \\ \phi_2^{(e)} \end{Bmatrix}$$

$$\Rightarrow \left(\frac{\mathrm{d}\phi}{\mathrm{d}s}\right)^{(e)}_{\text{AVE}} = \frac{1}{L^{(e)}} \lfloor -1\ \ 1 \rfloor \begin{Bmatrix} \phi_1^{(e)} \\ \phi_2^{(e)} \end{Bmatrix} \tag{15}$$

The scaling factor for the tangential derivative of the potential is obtained as

$$\mathrm{SF}_{\phi} = \frac{1}{N}\left[\sum_{(e)} \mathrm{SF}_{\phi^{(e)}}\right]^{1/2} \tag{16}$$

A similar procedure is performed to obtain the scaling factor for the tangential derivatives of the flux, SF_q, by replacing ϕ by q in the above equations. The element error with combined contributions from the tangential derivatives of both the potential and the flux is obtained as

$$E_{\phi+q^{(e)}} = \frac{E_{\phi^{(e)}}}{\mathrm{SF}_{\phi}} + \frac{E_{q^{(e)}}}{\mathrm{SF}_q} \tag{17}$$

The resulting local error $E_{\phi+q^{(e)}}$ with combined scaled contributions of ϕ and q is non-dimensional. The average error $E_{\phi+q_{\mathrm{AVE}}}$ and the normalized element errors $E_{\phi+q^{(e)}_{\mathrm{norm}}}$ are obtained by replacing ϕ by $\phi + q$ in the second and third equations of Equation (12).

2.2. The external domain approach for error estimation in BEM

Usually, error estimation approaches are most concerned with discretization error and seek an optimal adaptive procedure for mesh refinement. Among available methods, the difference between two equivalent formulations is one of the simplest. The exact solution for the BVP as written in one integral representation satisfies any other possible different integral representation of the same BVP. When a numerical solution is found for one formulation, this solution can be substituted into the discretized form (with same discretization) of the other possible formulation. Because numerical solutions are not exact, the identities in the discretized form of this second formulation will not be satisfied. The difference is a measure of the discretization error of both formulations.

For example, for a closed domain, the exterior boundary integral representation equals zero in both the potential and in the elastostatics problems. Thus, any difference from zero can be related to the discretization error. Because fundamental solutions are functions of the distance between source and field points, one representation in which the exterior point is very near the boundary might give a different error measure than the case in which the point is far away from the boundary. If different exterior points are considered, several external formulations may be obtained. The error measure is sensitive to the external point position for non-trivial problems.

In the present work, an error estimator is implemented for a 2D potential problem based on the fact that the potential vanishes at external points. A numerical solution at the boundary is first obtained for the discretized mesh using a collocation BEM formulation. This boundary solution is then substituted into the exterior form of Green's identity given by

$$-\int_S \phi(s)\vec{\nabla}\ln\left(\frac{1}{r(s,y)}\right)\cdot\vec{n}(s)\,\mathrm{d}S + \int_S \vec{\nabla}\phi(s)\cdot\vec{n}(s)\ln\left(\frac{1}{r(s,y)}\right)\mathrm{d}S = \phi(y) = E^{(e)}_{\mathrm{EXT}} \tag{18}$$

for $\forall y \in \bar{R}$ in a close vicinity to the boundary element (e). The absolute value of the error is taken so that local error information is always positive. Naturally, if the numerical boundary solution is exact, the exact Green's identity for the exterior point is obtained, and $\phi(y) = E^{(e)}_{\mathrm{EXT}} = 0$.

The exterior evaluation point $y \in \bar{R}$ is proposed to be located at a distance from the boundary (the distance from the exterior point to the nearest point on the boundary) that is a fraction α of the size of the boundary element nearest to this exterior point. This distance is measured from the element centre in the direction normal to the element at this point. In this work, numerical experiments are performed with various values of α in order to chose the most appropriate location for the external point y. As the external point approaches a boundary region, the error information becomes local. On the other hand, if the external point is too close to the boundary, numerical errors may appear due to a quasi-singularity problem. In Section 3, the element errors $E_{\mathrm{EXT}}^{(e)}$ for various values of α are compared. Comparisons are also made between $E_{\mathrm{EXT}}^{(e)}$ and $E_{\phi}^{(e)}$ to demonstrate the consistency of the local information given by these error estimators with mesh refinement.

3. IMPLEMENTATION OF THE PROPOSED ERROR ESTIMATORS

Two numerical examples of heat conduction are performed to demonstrate the implementation of the two proposed error estimators. The first problem involves a rectangular domain with two types of boundary conditions on one side. A discontinuity in the flux exists at the smooth intersection point between the two different types of boundary conditions. When discretizing the boundary, numerical errors are expected at the elements near the singular point because the boundary solution is not able to reproduce exactly the singular flux on one side of the singular point. The idea here is to verify if the error estimators can identify this boundary region as having higher local errors.

The second problem involves an axisymmetric pipe with curved boundary segments and a known analytic solution. This problem presents two special features due to the geometry and boundary conditions. The first feature is that in any radial boundary segment only the tangential derivatives of the potential and the flux change. The second feature is that on the circular arcs of the pipe boundary both the exact potential and the exact flux are constant; therefore their exact tangential derivatives are zero. The boundary elements (linear elements, in this study) do not preserve the circular arcs; therefore local errors are expected on the approximate boundary.

Depending on the boundary conditions, the flux at a corner node can be discontinuous. Local errors are expected in a vicinity of these corners as the numerical code evaluates the unknown discontinuous flux. All BEM results were obtained with the code BETIS presented in Paris and Cañas [32] with 12-point Gaussian integration. This code uses linear elements, but the error estimator procedures proposed in this work can use any degree in the element polynomial interpolants.

3.1. The Motz problem

The problem proposed by Motz [34] consists of a rectangular domain, as shown in Figure 1(a), in which a singularity exists at the point O ($s = 7$). The potential (temperature) is prescribed in the element to its left, and the flux equals zero in the element to its right. The flux is singular at point O in the element where the potential is prescribed.

Five meshes are considered to compare the error estimators. The coarsest mesh, with 10 elements, is shown in Figure 2(a). This mesh has only two elements in each linear segment

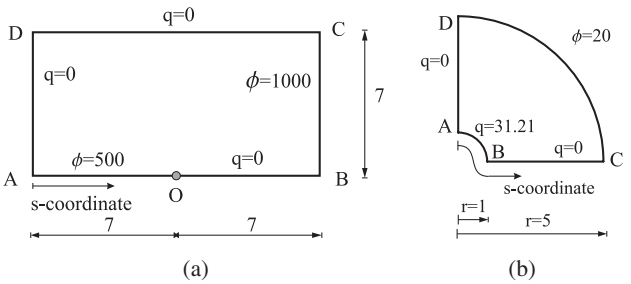

Figure 1. Numerical examples: (a) the Motz problem: a singularity is created at point O by the mixed boundary conditions; and (b) axisymmetric heat conduction in a pipe. One-quarter of the pipe cross-section is modelled.

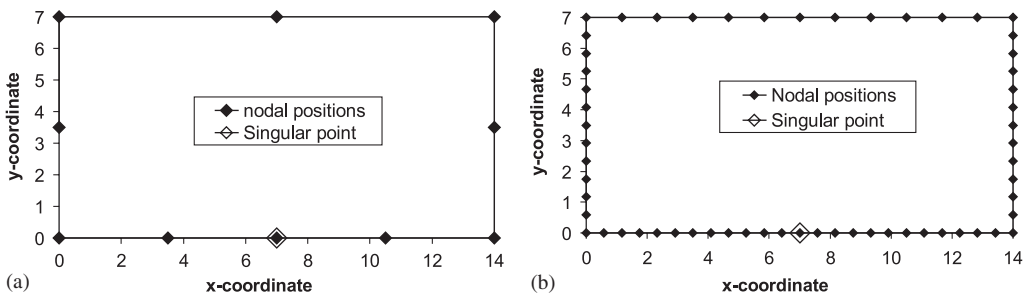

Figure 2. Meshes for the Motz problem: (a) coarse mesh: 10 elements; and (b) a finer mesh: 60 elements.

in which a uniform boundary condition is prescribed. The mesh with 20 elements is obtained dividing each element by two. Finer meshes are also studied to illustrate the general trend of the local errors with mesh refinement. The mesh with 60 elements is shown in Figure 2(b). The meshes with 120 and 240 elements are obtained subsequently by dividing each element by two.

Element matrices given by Equation (9) were assembled for the various meshes. For all meshes, the number of elements in the expanded system of equations includes the original elements plus four zero-length elements that were added at the boundary corners and one zero-length element that was added at the singular point, which is treated as a 'corner' because the flux is discontinuous at this point.

By solving the assembled system of equations, the vectors of nodal values for the smoothed tangential derivatives of the potential $\{\mathrm{d}\phi/\mathrm{d}s\}^{(e)*}$ and the flux $\{\mathrm{d}q/\mathrm{d}s\}^{(e)*}$ are obtained. The vector of element interpolations for the original non-zero elements is obtained from Equation (10). The residuals $r^2_{\phi^{(e)}}(\xi)$ and $r^2_{q^{(e)}}(\xi)$ are evaluated using Equation (11), and the element errors $E_{\phi^{(e)}}$ and $E_{q^{(e)}}$ are obtained using Equation (12) and compared with the local element errors $E^{(e)}_{\mathrm{EXT}}$, obtained using Equation (18).

3.1.1. Comparison of the error estimators results for the Motz problem. After the BEM solution is obtained for the boundary, the local error can be calculated for all elements using

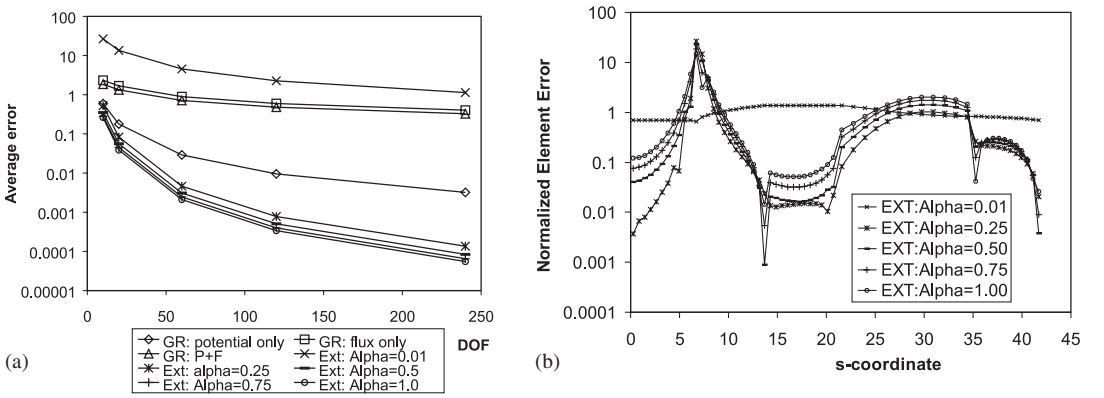

Figure 3. Motz problem: (a) average (global) error estimators for the gradient recovery (GR) procedure and for the external domain (Ext) approach for various values of α; and (b) influence of the position of the external point for the 60 elements mesh. Plotted error results for various values of α.

both the gradient recovery approach and the external domain approach. Several numerical results for the element error are obtained for the gradient recovery approach, including the recovery of the tangential derivatives for the potential only, for the flux only, and for a combination of both. The combined case is performed with scaling of the individual contributions of potential and flux given by Equation (17). Also, several numerical results are obtained for the external domain error estimator, using five values of α: $\alpha = 0.01$, 0.25, 0.5, 0.75 and 1.0.

The average of the element errors for each case gives an estimator for the global error associated with a particular discretization. Also, this average is used to normalize the element errors to facilitate their comparison. Figure 3(a) shows the behaviour of the average error as the mesh is refined. In all cases, the global error, as estimated by the average of the element errors, decreases with mesh refinement, showing the consistency of the error estimators.

The external error estimators, after being normalized by their average, are then compared for various distances from the exterior point to the boundary. Figure 3(b) illustrates the case for the mesh of 60 elements. The horizontal axes of the various plots corresponds to the s-co-ordinate of the middle of each element along the boundary, starting from the origin at point A (see Figure 1(a)). The co-ordinate of the singular point O is $s = 7$. The co-ordinates of the corner nodes A, B, C and D are $s = 0$ (and 42), 14, 21 and 35, respectively.

The error estimates in Figure 3(b) for $\alpha = 0.01$ are nearly constant. This case represents an external point very near the boundary, and apparently the numerical errors are primarily associated with the near-singularity of the integral equation evaluated at these points. As the distance from the boundary increases, local information on the boundary error becomes apparent. For example, for all values $\alpha \geqslant 0.25$, large errors near the singular point O exist.

When the value of α increases from 0.01 to 0.25 the relative differences in the element errors increase so that qualitative comparisons for the element error can be made. But when α continues its growth, the differences between the elements become smaller again. This phenomenon can be clearly seen, for example, in the region between corner nodes C and D, where the external error reaches its smallest value for $\alpha = 0.25$. When α increases, the error distribution starts losing its local character. For even larger values of α, the error information is expected to represent the global error only, with local differences completely attenuated.

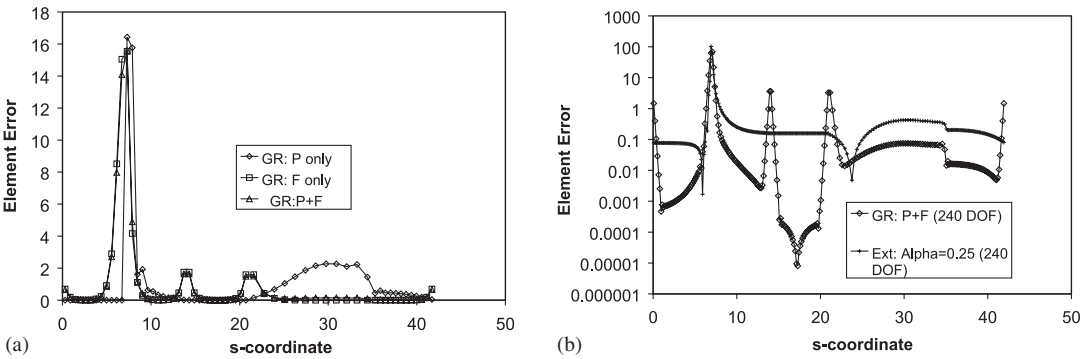

Figure 4. Motz problem: (a) Influence of the individual contributions of potential only (GR : P) and flux only (GR:F) for the gradient recovery (GR : P+F) error estimator for the 60 elements mesh; (b) comparison between gradient recovery (GR : P+F) and External ($\alpha = 0.25$) error estimators for the 240 elements mesh.

The external error estimator is based on the evaluation of the potential at the exterior point only, without any evaluation of the derivatives of the potential in any direction. But from Figure 3(b), this error estimator is capable of indicating the large errors in the vicinity of the singular point *O*, on both sides of this point. On the elements belonging to the side *AO*, the potential is prescribed and errors can only come from the calculated flux, and on the elements belonging to the side *OB*, the flux is prescribed and errors can only come from the calculated potential. Thus, the method appears to be insensitive to the type of boundary condition in the nearest element.

Figure 4(a) presents the results for three gradient recovery models: recovery of potential (GR : P only), recovery of flux (GR:F only), and recovery of both potential and flux (GR : P+F). Both the individual contributions (GR : P only and GR:F only) for the error estimator correctly identify high errors in the region near the singular point. The error from the potential (GR : P only) is higher in elements belonging to the side *OB*, and the error from the flux (GR:F only) is higher in elements belonging to the side *AO*. Also, only the error from the flux (GR:F only) predicts large error near corner nodes *B* and *C*. The relatively large errors from the potential (GR : P only) in the region near corner *D* are moderated when combined into the total error (GR : P+F) due to the difference in the averages of the individual contributions as shown in Figure 3(a).

Figure 4(b) shows a comparison between both error estimators for the finest mesh tested, with 240 elements. As expected, each estimator indicates the same region about the singular point *O* as having largest error. Also, both error estimators show similar qualitative behaviour in the vicinity of corner node *D*. But only gradient recovery (GR : P+F) was able to show the errors in the vicinity of corner nodes *B* and *C*. The error at these corner nodes originates from the flux that is calculated in one element sharing the node, while the potential and the flux in the other element are prescribed at this node.

Figure 5(a) shows results for the gradient recovery error obtained when combining the recovery of the tangential derivatives of both the potential and the flux (GR : P+F), for various meshes. These results are qualitatively comparable and consistent as the mesh is refined. Similarly, Figure 5(b) shows results for the error obtained using the exterior domain

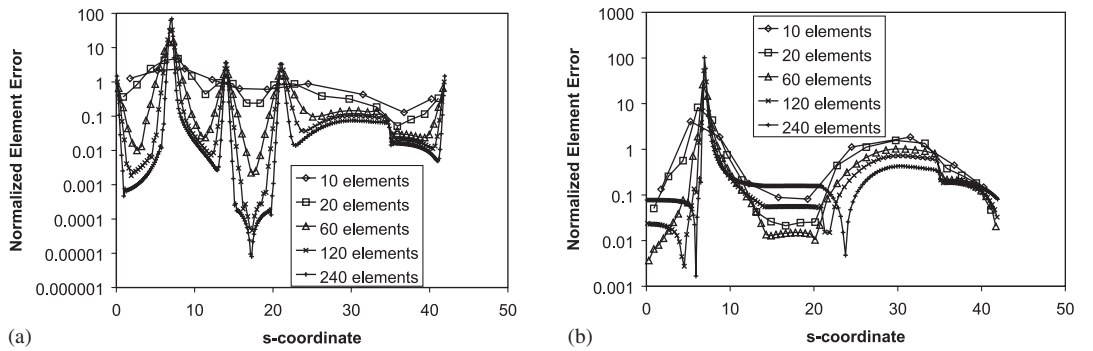

Figure 5. Motz problem: influence of mesh refinement for: (a) the gradient recovery (GR) error estimator with potential and flux combined; and (b) the external domain (Ext) error estimator with $\alpha = 0.25$.

formulation with $\alpha = 0.25$. Again, the error results are qualitatively consistent with the mesh refinement.

The boundary region immediately before corner node *D* produces relatively high errors when considering the external error as in Figure 3(b). These error results are also obtained for the gradient recovery error with recovery of the tangential derivative of the potential (GR : P only) as in Figure 4(a). These errors occur because this region is farthest from any boundary where the potential is prescribed. Both error estimators rely on the evaluation of the potential. The gradient recovery approach relies on the evaluation of the tangential derivative of the boundary potential using the interpolating functions, while the exterior domain approach relies on the evaluation of the potential at an exterior point. This evaluation is highly influenced by the potential at the boundary points closest to this external evaluation point, and therefore larger errors are expected in regions far from other boundary regions where the potential is prescribed.

We also note that, because the element before the singular point has a prescribed potential, any contribution to the error can only originate from error in the flux. This feature can be seen in Figure 4(a), where the larger contribution to the total gradient recovery error (GR : P+F) is the recovery of the flux (GR:F only). Similarly, the element after the singular point has a constant prescribed flux. Any contribution to the error can only originate from the error in the potential in this element. Again, this result can be seen in Figure 4(a), where most of the contribution to the total gradient recovery error (GR : P+F) comes from the recovery of the potential (GR : P only).

An important point to note from Figure 4(a) is that only the error estimator with recovery of the flux (GR:F only) is capable of identifying the relatively high errors in the vicinity of corner nodes *B* and *C*. As seen in Figure 3(b), the external error estimator predicts a jump in the error at these corner nodes—almost a step in the error as a function of the *s*-co-ordinate—but is not capable of isolating properly the local error or of showing that this local error is concentrated in a vicinity of these corner nodes.

3.2. The pipe problem

This example illustrates the use of the two error estimators for steady-state heat conduction in a pipe. By symmetry, only one quarter of a pipe is considered, as shown in Figure 1(b). The body is one quarter of a two-dimensional disk with flux prescribed on the inner circular

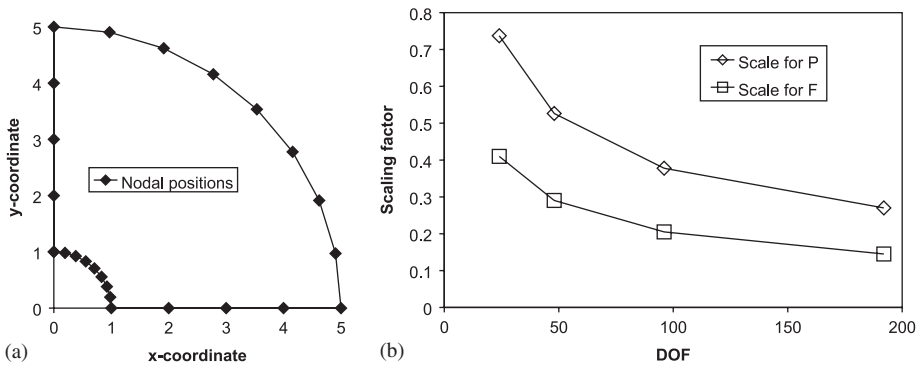

Figure 6. Pipe problem: (a) coarse mesh: 24 elements; and (b) scaling factors for the gradient recovery (GR : P+F) error estimator. Individual contributions of the potential (P) only and of the flux (F) only are scaled before combined to give the GR : P+F error estimator.

boundary, insulated (zero flux) along the radial (rectilinear) edges, and temperature specified on the outer circular boundary. The inner radius is 1.0 and the external radius is 5.0. The flux at the inner circular boundary is 31.21 units and the temperature at the external circular boundary is 20.0 units. The thermal conductivity is $k = 1$.

In this problem, radial symmetry produces an ordinary differential equation $\mathrm{d}^2\phi/\mathrm{d}r^2 + 1/r\,\mathrm{d}\phi/\mathrm{d}r = 0$, whose exact solution is $\phi(r) = 31.21\ln(9.490/r)$ for the potential and $q(r) = -31.21/r$ for the flux. The exact temperature at the inner circular boundary is 70.231, and the exact flux at the outer circular boundary is -6.242.

Several meshes were constructed to evaluate the error estimators for this problem. The coarsest mesh, with 24 elements, is shown in Figure 6(a). Each straight line segment of the boundary has four elements, while each arc is composed of 8 elements. Finer meshes with 48, 96 and 192 elements are obtained subsequently by dividing each element by two in each mesh refinement step.

3.2.1. Comparison of the error estimators results for the pipe problem. After the boundary solution is obtained using the BEM code, the local element error is calculated using both the gradient recovery and the external domain approaches. Several categories of element error are obtained for the gradient recovery approach. Recovery of the tangential derivatives is performed for the potential (GR: P only), for the flux (GR:F only), and for a combination of both (GR : P+F), with scaling of the individual contributions of potential and flux given by Equation (17). The scaling factors evaluated for the various discretizations are plotted in Figure 6(b). Also, several numerical results are obtained for the external domain error estimator, with: $\alpha = 0.01,\ 0.25,\ 0.5,\ 0.75$ and 1.0.

The average of the element errors for each case gives an estimate of the global error associated with a particular discretization. Also, this average is used to normalize the element errors for their comparison. Figure 7(a) shows the behaviour of the average error for the various cases tested as the mesh is refined. The average errors of the nodal solution with respect to the known exact boundary solution are also included. In all cases, the global error decreases with mesh refinement and demonstrates the consistency of the error estimators. This behaviour of the average estimated error is also consistent with the exact error.

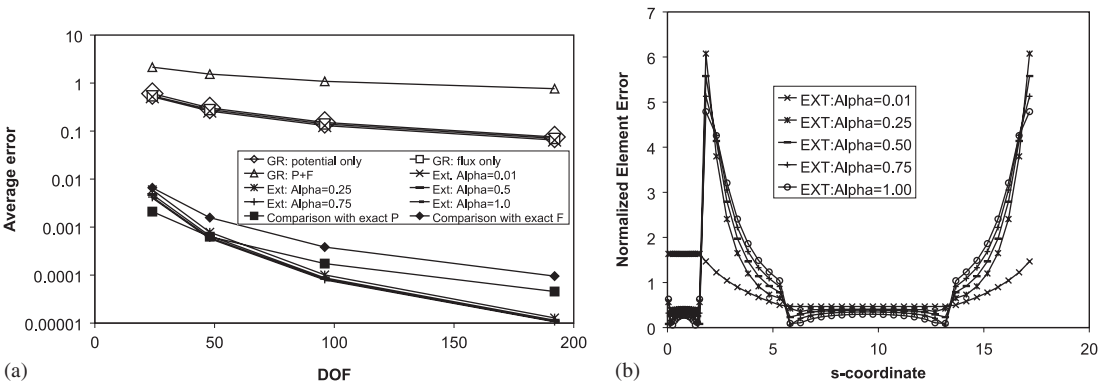

Figure 7. Pipe problem: (a) average (global) error estimators for the gradient recovery (GR) procedure and for the external domain (Ext) approach for various values of α. Also included the errors with respect to the known exact boundary solution; and (b) influence of the position of the external point for the 48 elements mesh. Plotted error results for various values of α.

The normalized external error estimators have been compared for various distances from the exterior point to the boundary. Figure 7(b) illustrates the results for a mesh of 48 elements. The origin of the s-co-ordinate is point A (see Figure 1(a)). The co-ordinates of the corner nodes A, B, C and D are $s = 0$ (and 17.42), 1.57, 5.57 and 13.42, respectively.

The error results for $\alpha = 0.01$ present the least variation of all cases. This case represents an external point very near the boundary, and apparently the numerical errors are primarily associated with the near-singularity of the integral equation evaluated at these points. When the value of α increases from 0.01 to 0.25, the relative differences in the element errors increase, so that qualitative comparisons for the element error can be made. But when α continues to increase, the differences between the elements become smaller again because the local information becomes attenuated. This phenomenon can be clearly seen, for example, for the elements nearest to corner nodes A and B on the straight part of the boundary, where the external error reaches its highest value for $\alpha = 0.25$. When α increases, the error information begins to lose its local character. For even larger values of α, the error information is expected to represent the global error only, with local differences completely attenuated.

Figure 8(a) presents the contributions from recovery of potential (GR : P only), recovery of flux (GR:F only), and the total gradient recovery error estimator (GR : P+F). Both the individual contributions (GR : P only and GR:F only) identify the high errors on the region near the corner nodes A and B on the straight part of the boundary. In this region, the exact result for the error in the boundary potential is high, as seen in Figure 8(b). Also, only the error from the flux (GR:F only) predicts high errors near corner nodes C and D, where the exact result for the error in the boundary flux is high, as seen in Figure 8(b).

Figure 8(b) provides a comparison between both error estimators for the same mesh with 48 elements. The plots for the exact error for the boundary potential and for the boundary flux are also included. Both error estimators exhibit similar qualitative behavior in the vicinity of the corner nodes A and B on the straight part of the boundary, where large errors occur as expected. But only the error estimator from gradient recovery (GR : P+F) shows high errors in the vicinity of corner nodes C and D. The error at these corner nodes comes from the flux

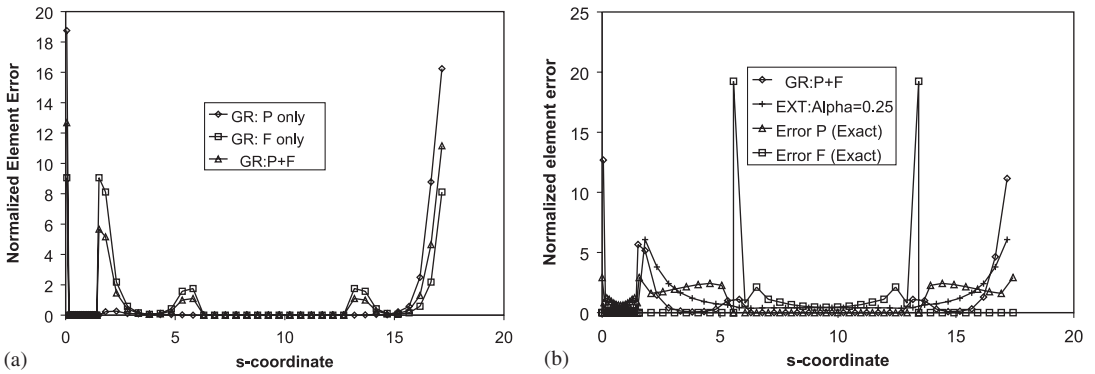

Figure 8. Pipe problem: (a) influence of the individual contributions of potential only (GR : P) and flux only (GR:F) for the gradient recovery (GR : P+F) error estimator for the 48 elements mesh; and (b) comparison between gradient recovery (GR : P+F) and External ($\alpha = 0.25$) error estimators for the 24 elements mesh. Also included the errors with respect to the known exact boundary solution.

that is calculated in one element sharing the node because the potential and the flux in the other element is prescribed at this node.

An important point to note from Figure 8(a) is that, similarly to the Motz problem, only the error estimator with recovery of the flux (GR:F only) is capable of identifying the relatively high errors in the vicinity of corner nodes *C* and *D*. As seen in Figure 7(b), the external error estimator is capable of showing a steep change in the error at these corner nodes—almost a step in the error as a function of the *s*-co-ordinate—but is not capable of isolating properly the local error, or of showing that this local error is concentrated in a vicinity near these corner nodes.

Similarly to the Motz problem, a comparison for the error estimators with mesh refinement was performed. Error estimator results were obtained for the combined gradient recovery error (GR : P+F) and for the exterior domain formulation for $\alpha = 0.25$ for various meshes, with 24, 48, 96 and 192 elements. Again, these results were qualitatively comparable and consistent with the mesh refinement. No figure with this comparison is included here.

3.3. *Summary of error results*

The global error estimators obtained from the average of both the gradient recovery error estimator (GR : P+F) and the external domain error estimator (Ext: $\forall\alpha$) are qualitatively comparable and consistent with mesh refinement. Regarding qualitative local error information, some differences exist between the error estimators. Both error estimators (GR : P+F and EXT for $\alpha \geqslant 0.25$) were comparable and capable of recovering local error information for the case of high errors due to singularities in the boundary solution (regardless of the error source) and for the case where the error source is primarily the potential.

However, the exterior domain approach was not able to describe correctly local errors when the error source is primarily the flux, such as corner nodes where the potential and flux on one side of the node are prescribed. In this case, only the gradient recovery approach (GR : P+F) can identify correctly the local region that is in error.

The relative contributions to local error from the potential and from the flux is problem-dependent. For some cases in which the effect of the boundary curvature is small, the most important contribution to the local error could derive from the tangential derivative of the potential, as discussed in Jorge *et al.* [35]. In the Motz problem, this effect is evident in boundary regions far from the singular point. In the pipe problem, this effect is evident on the straight sides of the boundary. The error estimator using the gradient recovery approach (GR : P+F) provides local error information that is less problem-dependent than approaches based on potential (GR: P only) and flux (GR: F only).

Finally, another positive point for the gradient recovery error estimator (GR : P+F), which contributes to its generality of use, is that the estimator is not dependent on any *ad hoc* parameter. Conversely, the external error estimator depends on an appropriate choice of the distance from the external point to the boundary. If this distance is too small, the external error information is primarily derived from near-singularities of the integral formulation, and no local information can be extracted for the boundary error. If this distance is too large, the error information may lose its local character, and the error information tends to become more of a global error type. The choice of the optimal parameter α may be problem-dependent and also mesh-dependent. For a particular problem, coarse meshes might require smaller values of α for the error to keep its local character. On the other hand, fine meshes might require larger values of the parameter α in order for the distance to the boundary to be sufficiently large for the numerical errors due to the near-singularities not to become dominant. For the cases tested, $\alpha = 0.25$ gave reasonably good results for the potential-related error for all meshes.

4. ADAPTIVE MESH REFINEMENT USING A LOCAL ERROR ESTIMATOR

Local measures of discretization error in each element can be compared to an average global measure of this error. If the relative error is greater than unity for a certain element, refinement may be appropriate for this element. Adaptive refinement of the mesh could be performed by adopting *h*-refinement or *p*-refinement procedures. In the *h*-refinement procedure, the element where the local error is large is divided into two small elements (usually of equal length). In the *p*-refinement procedure, the degree of the shape functions used to represent the variables in this element is increased. For this *p*-refinement procedure, the use of hierarchical shape functions is advantageous because computations already performed for the coarse mesh do not need to be evaluated again in the refined mesh. Another approach involves distortion of the mesh in order to obtain smaller error without increasing the number of degrees of freedom of the problem. This *r*-refinement procedure seeks to distribute the local error equally throughout the boundary without increasing the number of nodes or the order of the interpolating polynomials.

An adaptive *r*-refinement procedure is proposed here. The goal is to minimize the variability of the element error, and a function representing the standard deviation of this error can be constructed. This procedure can be applied using any local error estimator, such as those described in Sections 2.1 and 2.2. In what follows, an error estimator for the external problem with $\alpha = 0.25$ is adopted to obtain the local error results.

The same numerical example proposed by Motz [34] and detailed in Section 3 is now used to demonstrate of the adaptive *r*-refinement procedure. The first mesh is coarse and has only two elements in each linear segment in which a uniform boundary condition is prescribed,

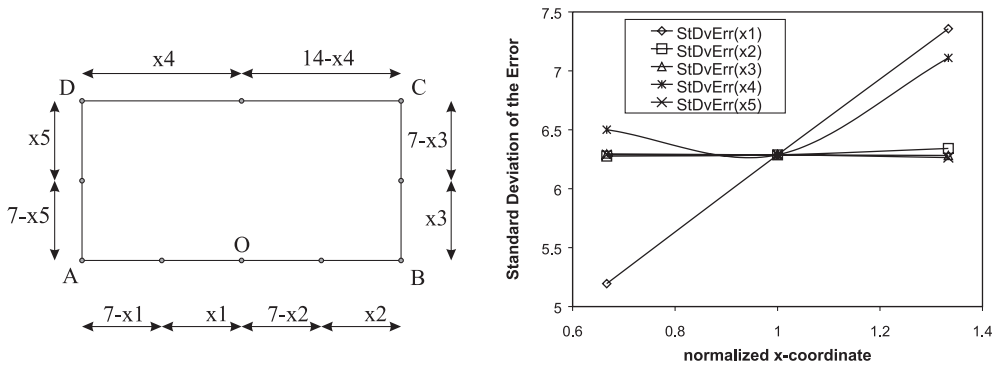

Figure 9. Coarse mesh: (a) the variables $x1$, $x2$, $x3$, $x4$ and $x5$ correspond to the position of the interior nodes in each linear segment AO, OB, BC, CD and DA. Position of interior nodes can vary separately; and (b) sensitivity of the standard deviation of the element error with element size variations in different regions of the boundary. Horizontal axis is a normalized x-co-ordinate given by $x_i/(x_i)_{(\text{initial})}$, for $i = 1, 2, 3, 4, 5$.

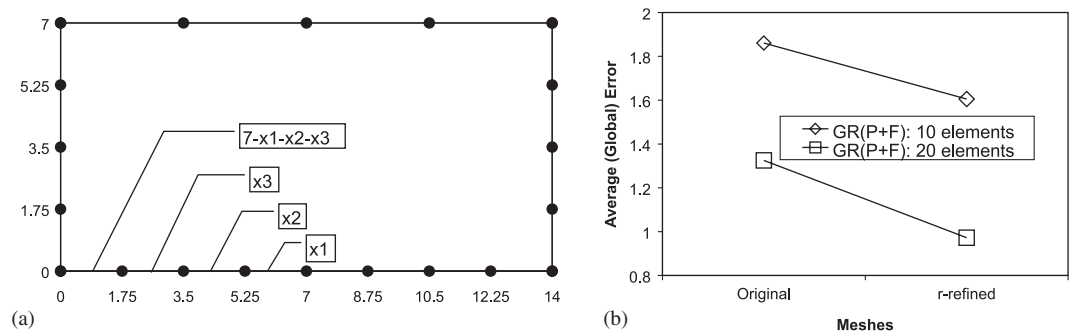

Figure 10. (a) Finer mesh: The variables $x1$, $x2$ and $x3$ correspond to the position of the 3 nodes internal to the linear segment AO. Position of these nodes can vary separately; and (b) influence of r-refinement for the coarse and fine meshes, measured by the average (global) gradient recovery error estimator with potential and flux combined (GR : P+F).

as shown in Figure 9(a). This coarse mesh illustrates the general trend of the optimization procedure. Then, a finer mesh is studied in which eight elements exist on the side where the flux is discontinuous. This finer mesh is obtained by dividing each element of the coarse mesh by two, as shown in Figure 10(a). For this mesh, a non-linear constrained optimization procedure is implemented using a feasible-point method as described by Nash and Sofer [36].

After the BEM solution is obtained for the boundary, the local error is evaluated for all elements using the external domain approach. From the distribution of errors, the average and the standard deviation can be calculated. The average represents a measure of the global error. The complete procedure for finding the optimal mesh so that the error is minimal with a small

number of nodes in the mesh requires two steps. The first step is to make the distribution of the local error as uniform as possible. This so-called *r*-refinement is accomplished by minimizing the variance of the error. The result is a distorted mesh in which the error is as equally distributed as possible. Then, in the second step, all elements are divided by two in a *h*-refinement procedure. Solution accuracy increases at every *h*-refinement step. The previous *r*-refinement step, even if not guaranteeing that the total error will be small, ensures that the element sizes are the ones that improve the distribution of error. The *r*-refinement procedure produces small elements in boundary regions where the local error was originally high and large elements where the local error is less sensitive to element size. In the subsequent *h*-refinement, the error function will be minimized using fewer nodes than would be needed if only *h*-refinement were employed.

4.1. Implementation of the r-refinement procedure for a coarse mesh

Starting from the mesh with 10 elements, various meshes were generated by varying the position of the nodes internal to the sides *AO*, *OB*, *BC*, *CD* and *DA*. Figure 9(a) shows this coarse mesh and also the variables representing the position of the nodes internal to the various sides. One side of the boundary is considered here as a linear segment having fixed nodes as the end points, and having just one type of boundary condition specified on it. Nodes are shown in Figure 9(a) in their initial positions, with the interior node at the centre of each side. The positions of interior nodes can change to minimize the error function.

The variables $x1$, $x2$, $x3$, $x4$ and $x5$ corresponding to the position of the interior nodes can vary separately. The default position of the interior nodes is in the middle of the line segments. A constraint was established so that the ratio between the sizes of two adjacent elements is at least $\frac{1}{2}$ and at most 2, to avoid numerical problems that might appear due to poor conditioning of the matrices in the BEM method.

A plot of the variance of the error is then obtained as a function of each variable separately as shown in Figure 9(b). The minimization procedure assumes, for simplicity, that the error varies independently with respect to all variables. The minimizer corresponding to the optimal position of the nodes for this mesh is obtained directly by observing the minimum value of all curves in the feasible range of the corresponding variables. The minimizer is $\{x1, x2, x3, x4, x5\}_* = \{2.333, 2.333, 4.667, 6.243, 4.667\}$.

Starting from initial values $\{x1, x2, x3, x4, x5\}_0 = \{3.5, 3.5, 3.5, 7.0, 3.5\}$, convergence was monotonic to one of the interval bounds for all variables except $x4$, for which the minimum of the objective function was inside its range of variation. As expected, the procedure produced smaller elements near the singular point.

Comparison of the various plots in Figure 9(b) highlights the sensitivity of the standard deviation of the error with respect to element size variation for the various regions of the boundary. The sensitivity of the standard deviation for variations in the region *AO* (elements of size $(7 - x_1)$ and x_1) is the highest, followed by the region *CD* (elements of size $(14 - x_4)$ and x_4). Variations of the nodal positions x_3 and x_5 produce only very small changes in standard deviation. This result is compatible with results for the external domain error estimator presented in Figure 3(b).

The boundary regions that presented the highest values of the element error also presented the highest values of sensitivity for changes in nodal position, i.e. in element size. The secondary errors close to corner *D* in region *CD* are associated with the secondary sensitivity

for the variation of x_4. The lowest values of the element error in the regions BC and DA are associated with the lowest sensitivity for the variation of x_3 and x_5, respectively. Apparently, only the relatively high errors near the singular point O in region OB (which are of the same order as those close to point O in region AO) are not directly associated with the sensitivity to the variation of x_2, which is small compared to the sensitivity with the variation of x_1.

The sensitivity of the standard deviation of the error with respect to element size variation appears to be a promising alternative to check and validate the results obtained with a local error estimator. Also, the sensitivity analysis is useful to determine the boundary regions in which remeshing should preferably be performed (high sensitivity regions) and the regions where remeshing is less important (low sensitivity regions). For example, for the present problem, the sensitivity analysis shows that remeshing could be done, with satisfactory results, on region AO only (i.e. varying x_1 only), as the other variables contribute very little to the reduction in the standard deviation of the error. This procedure is adopted for the next case study of a finer mesh.

4.2. Implementation of the r-refinement procedure for a refined mesh

4.2.1. Obtaining the objective function. Based on the sensitivity analysis of the error results for the coarse mesh in Figure 9(b), an r-refinement procedure for a refined mesh with 20 elements is performed by varying the position of the nodes on side AO only. This side is the part of the boundary that contains the singularity in the flux and also is the side in which the standard deviation of the error presented the highest variation when the relative size of the elements was changed. In a more general problem, this procedure could be adopted for all sides of the boundary. Figure 10(a) shows this finer mesh and also the variables representing the position of the nodes internal to side AO. The results for the standard deviation of error are approximated by a quadratic function in the form

$$\begin{aligned}\mathrm{StDvErr}(x1,x2,x3) = {} & c_{11}x_1^2 + c_{22}x_2^2 + c_{33}x_3^2 + c_{12}x_1x_2 + c_{13}x_1x_3 \\ & + c_{23}x_2x_3 + c_1x_1 + c_2x_2 + c_3x_3 + c_0 \end{aligned} \tag{19}$$

The choice of a quadratic objective function $f(x)$ derives from the simplicity of its being the lowest possible degree for a polynomial that admits non-zero second-order derivatives. Thus, its Hessian matrix $\nabla^2 f(x)$ is not identically zero *a priori*, as would be the case for a linear objective function, for example. A point x_* satisfying the first-order necessary condition for a minimizer ($\nabla f(x_*) = 0$) is a stationary point of the function f. This point x_* is a strict local minimizer if the second-order sufficient condition ($\nabla^2 f(x_*)$ is positive definite) is also satisfied [36].

The procedure to obtain this second-degree approximation is outlined from a design of experiments (DOE) approach. For the three variables $\{x1,x2,x3\}$, it would be necessary to evaluate the solution for 27 different combinations to obtain an approximation considering all the interactions between the variables. Instead, a partial design is adopted, as follows. Starting from the middle point, a cube is obtained by varying the nodal positions as shown in Figure 11 (left). Six other evaluation points are obtained, corresponding to the centres of the cube faces. But to approximate the function by a quadratic function, 10 points are necessary to generate all coefficients. The extra three points are obtained assuming three likely situations:

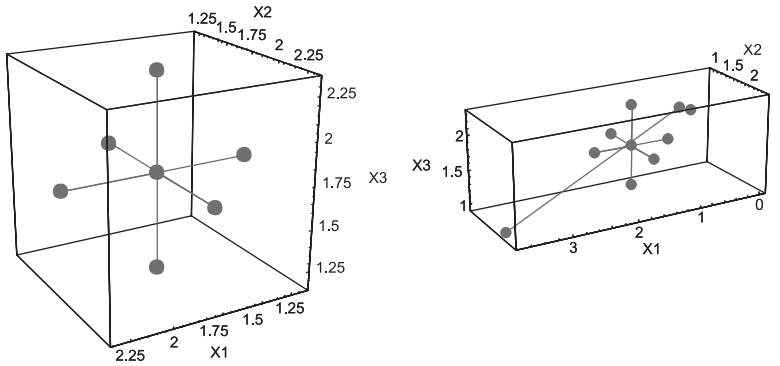

Figure 11. Position of the points in the adapted partial central design of experiments (DOE) approach.

either all points move to the right, all points move to the left, or the points closer to the segment ends move each to the corresponding end of the segment.

A typical display of the DOE points would be a cube, with points at the ends, at the centre of the edges, at the centre of the faces, or at the centre of the cube. Each side of the cube corresponds to the range of one of the variables, $x1, x2, x3$. In this case, the final design is not a cube because of the last three points added. The position of the 10 points chosen to evaluate the value of the objective function is shown in Figure 11 at the right. The objective function coefficients were evaluated by solving the linear system of ten equations, obtained with the values of the objective function evaluated for all 10 points.

$$\begin{aligned}\mathrm{StDvErr}(x1,x2,x3) = {} & 0.0583898x_1^2 - 0.0013669x_2^2 + 0.000214617x_3^2 + 0.199897x_1x_2 \\ & + 0.142247x_1x_3 + 0.362173x_2x_3 - 0.0895247x_1 - 0.966685x_2 \\ & - 0.887556x_3 + 4.31078 \end{aligned} \tag{20}$$

4.2.2. Nonlinear constrained optimization procedure: feasible-point method. The constraints on the ratio of the element sizes are the same as those used in the coarse mesh study. The ratio of the sizes of any two adjacent elements must not exceed 1 : 2 to avoid numerical errors. For the side being evaluated, this requirement produces a set of six inequality constraints:

$$\begin{aligned} & g1(x1,x2,x3) = 2x_2 - x_1 \geqslant 0, && g2(x1,x2,x3) = 2x_1 - x_2 \geqslant 0 \\ & g3(x1,x2,x3) = 2x_3 - x_2 \geqslant 0, && g4(x1,x2,x3) = 2x_2 - x_3 \geqslant 0 \\ & g5(x1,x2,x3) = -2x_1 - 2x_2 - 3x_3 \geqslant -14, && g6(x1,x2,x3) = x_1 + x_2 + 3x_3 \geqslant 7 \end{aligned} \tag{21}$$

A feasible-point method was chosen to solve the optimization problem. This procedure is described by Nash and Sofer [36]. Among the constraints, some are chosen as active so that the optimization problem for the objective function will have these active constraints as equality constraints, and, thus, Lagrange multipliers can be used. This procedure allows the

evaluation of only some combinations of the constraints as active. Whenever the boundary of another constraint is reached, this constraint is added to the active set. If one of the Lagrange multipliers becomes negative, the corresponding constraint function is dropped from the working set.

The active set used in this work is adapted from Reference [36], and an outline is included here for clarity. A feasible starting point $x_k = x_0$ is assumed, and W is the index set of the active constraints at x_0. $\bar{A}$ represents the constraint matrix for the active constraints. Z is a null-space matrix for $\bar{A}$, and $\bar{A}_r$ is a right inverse for $\bar{A}$. The first step in the algorithm is to perform the optimality test, which consists of checking if $Z^T \nabla f(x_k) = 0$. Then the set of constraints is analysed. If no constraints are active, then the current point is a local (unconstrained) stationary point, and the algorithm stops. On the other hand, if active constraints exist, the Lagrange multipliers are computed as $\bar{\lambda} = \bar{A}_r{}^{\mathrm{T}} \nabla f(x_k)$, and their sign is tested. If $\bar{\lambda} \geqslant 0$, then the algorithm stops, because a local stationary point has been reached. Otherwise, a constraint corresponding to a negative multiplier from the active set is dropped, and the matrices W, $\bar{A}$, Z and $\bar{A}_r$ are updated.

The second step in the algorithm is to compute the search direction, which is a descent direction p that is feasible with respect to the constraints in the working set. The third step is to compute a step length satisfying $f(x_k + \alpha p) < f(x_k)$ and $\alpha \leqslant \bar{\alpha}$, where $\bar{\alpha}$ is the maximum feasible step along p. The fourth and last step in the algorithm is to find the new updated solution point $x_{k+1} = x_k + \alpha p$. At this point, if a new constraint boundary is encountered ($\alpha = \bar{\alpha}$), this constraint is added to the working set, and the matrices W, $\bar{A}$, Z and $\bar{A}_r$ are updated accordingly. The algorithm proceeds returning to the first step with $k = k + 1$ and is repeated until convergence is attained.

In this particular problem, the unconstrained minimization problem for the objective function has no solution because the Hessian matrix for this function has one eigenvalue that is negative. Therefore, the unconstrained problem does not satisfy necessary and sufficient conditions to have a minimizer, although it can have stationary points (e.g. saddle points).

It is important to make a good choice of the initial working set of constraints because this choice can reduce the number of calculations. For this particular problem, the three extra points in the design of experiments approach can be used to establish initial working sets. If all points move to the right, the working set is $W = \{g2, g4, g6\}$. If all points move to the left, the working set is $W = \{g1, g3, g5\}$. If the nodes close to the extremes move towards these extremes, with the central node remaining in the same position, then the working set is $W = \{g2, g5\}$. For this particular problem, the nodes are expected to move towards the singular point. Indeed, this behaviour was already observed for the coarse mesh. But this procedure shall be as general as possible, without using any clues from the specific problem. All three possibilities of initial working set are to be considered. When a stationary point is found, the second-order necessary and sufficient conditions are used to determine whether or not the solution is a minimizer. If it is, then the algorithm stops. If it is not, then it restarts with another initial working set until a minimizer is found.

The first working set to start the optimization procedure is taken to be the set corresponding to the lowest value of the error obtained in the design of experiments procedure. In this case, the working set is $W = \{g2, g4, g6\}$ which corresponds to the starting point $\{x1, x2, x3\}_0 = \{1.4, 2.8, 5.6\}/3 = \{0.47, 0.93, 1.87\}$. Starting with this working set, it was found that $g6$ should be eliminated. Then, the solution was found in one step only, as shown in

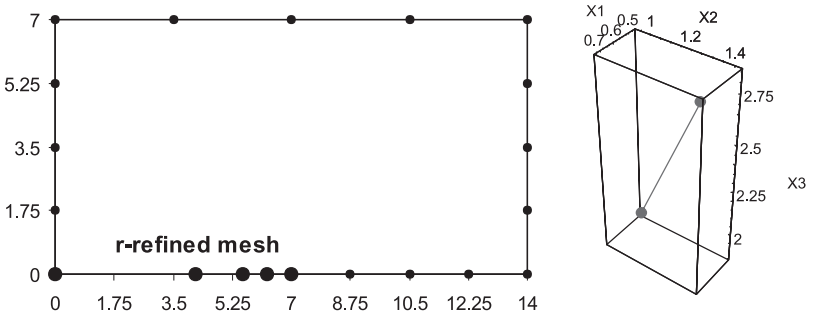

(a) (b)

Figure 12. Solution of the optimization procedure. Minimizer is $\{x1, x2, x3\}_* = \{0.71, 1.42, 2.84\}$: (a) smaller elements are obtained near the singular point; and (b) solution is obtained in one step only starting from the point $\{x1, x2, x3\}_0 = \{0.47, 0.93, 1.87\}$, corresponding to the working set $W = \{g2, g4, g6\}$.

Figure 12(b). The second-order necessary and sufficient conditions for this point to be a minimizer were confirmed; therefore this point is in fact a minimizer for the original function with the current working set. The minimizer is the point $\{x1, x2, x3\}_* = \{0.71, 1.42, 2.84\}$, and the minimum value of the objective error function is 2.33. Again, the procedure shifted the nodes towards the singularity point, as expected.

In a general situation, some uncertainty might exist concerning the initial working set of constraints. When reaching a stationary point, the second-order conditions must be checked to determine whether or not the point is a minimizer. If not, the problem is restarted with another set of active constraints. To amplify this point, the problem was started again but with $\{g2, g5\}$ as the initial working set. The procedure drops $g5$ and adds $g6$ to the working set. Then, with $g2$ and $g6$ in the working set, a stationary point is found at $\{x1, x2, x3\} = \{1.07, 2.14, 0.014\}$. But this point is not a minimizer because the necessary and sufficient conditions are not satisfied, and the value of the objective function at this point is larger than previously observed values.

Figure 10(b) shows a plot of the average (global) error evaluated for both meshes before and after the r-refinement procedure. Average errors are plotted for the gradient recovery error estimator (GR : P+F). Equivalent results were also found for the external error estimator (Ext : $\alpha = 0.25$). In both cases, the global error is smaller, for a particular number of DOF, after the nodes are re-positioned using this r-refinement procedure.

5. CONCLUSIONS

Two local error estimation techniques involving (1) gradient recovery of tangential derivatives and (2) an external problem formulation have been derived, implemented and compared for 2D BEM potential problems. These two error estimators represent a post-processing step, after the BEM solution is already known. Knowledge of the exact solution is not required for either error estimator. The results for the global error as obtained from both error estimators were qualitatively comparable and consistent as the mesh was refined.

Both error estimators were found to be comparable and capable of providing local error information for a case with singularities in the boundary solution and for the case in which the error source is dominated by the potential. In these cases, both error estimators identified the same boundary regions with the highest values for normalized error.

The error estimator from the exterior domain approach was not able to describe correctly local errors for the case in which the error source is primarily the flux, such as in the case of corner nodes with certain boundary conditions. In this case, only the gradient recovery approach (GR : P+F) can predict correctly the local region that is in error.

The gradient recovery error estimator (GR : P+F) does not depend on any *ad hoc* parameter, while the external error estimator depends on an appropriate choice of the relative distance α from the external point to the boundary. The choice of the parameter α may be problem-dependent and also mesh-dependent. For the cases tested, $\alpha = 0.25$ gave reasonably good results.

An adaptive *r*-refinement procedure to minimize variation of local error throughout the boundary was presented. The procedure was based on the minimization of the standard deviation of local error estimate. Inequality constraints for the nodal positions were used, and the objective function was obtained using design of experiments techniques. A non-linear programming procedure using a feasible-point method was adopted based on the use of Lagrange multipliers and a set of active constraints. The optimization procedure produced finer meshes near the singular point – a result that is consistent with the usual mesh generation procedures for this type of problem. This *r*-refinement procedure generates a distorted mesh that can be used as the starting point for subsequent *h*- or *p*-refinements. The sensitivity of the standard deviation of the error with respect to element size variation for the various regions of the boundary is compatible with the local error estimator results. The sensitivity analysis is useful to determine the boundary regions in which remeshing should preferably occur.

Future work on this topic could include the extension of the two error estimators for higher order elements for 2D potential and elastostatics problems.

ACKNOWLEDGEMENTS

The first two authors acknowledge the support received from CNPq—Conselho Nacional de Desenvolvimento Científico e Tecnológico and from FAPEMIG—Fundação de Amparo à Pesquisa do Estado de Minas Gerais. The third author gratefully acknowledges support by the National Science Foundation (CTS-9983961).

REFERENCES

1. Liapis S. A review of error estimation and adaptivity in the boundary element method. *Engineering Analysis with Boundary Elements* 1994; **14**:315–323.
2. Kita E, Kamiya N. Recent studies on adaptive boundary-element methods. *Advances in Engineering Software*, 1994; **19**:21–32.
3. Kita E, Kamiya N. Error estimation and adaptive mesh refinement in boundary element method, an overview. *Engineering Analysis with Boundary Elements* 2001; **25**:479–495.
4. Kelly DW, Mills RJ, Reizes JA. *A posteriori* estimates of the solution error caused by discretization in the finite element, finite difference and boundary element methods. *International Journal for Numerical Methods in Engineering* 1987; **24**:1921–1939.
5. Carstensen C, Stephan EP. A-posteriori error-estimates for boundary-element methods. *Mathematics of Computation* 1995; **64**(210):483–500.
6. Carstensen C, Estep D, Stephan EP. h-adaptive boundary-element schemes. *Computational Mechanics* 1995; **15**(4):372–383.

7. Carstensen C, Stephan EP. Adaptive boundary element methods for some first kind integral equations. *SIAM Journal on Numerical Analysis* 1996; **33**(6):2166–2183.
8. Carstensen C. Efficiency of a posteriori BEM-error estimates for first-kind integral equations on quasi-uniform meshes. *Mathematics of Computation* 1996; **65**(213):69–84.
9. Liang MT, Chen JT, Yang SS. Error estimation for boundary element method. *Engineering Analysis with Boundary Elements* 1999; **23**:257–265.
10. Paulino GH, Gray LJ, Zarikian V. Hypersingular residuals—a new approach for error estimation in the boundary element method. *International Journal for Numerical Methods in Engineering* 1996; **39**:2005–2029.
11. Menon G, Paulino GH, Mukherjee S. Analysis of hypersingular residual error estimates in boundary element methods for potential problems. *Computer Methods in Applied Mechanics and Engineering* 1999; **173**: 449–473.
12. Paulino GH, Gray LJ. Galerkin residuals for adaptive symmetric–Galerkin boundary element methods. *Journal of Engineering Mechanics* (ASCE) 1999; **125**(5):575–585.
13. Denda M, Dong YF. An error estimation measure in the direct BEM formulation by the external Somigliana's identity. *Computer Methods in Applied Mechanics and Engineering* 1999; **173**:433–447.
14. Jou J, Liu J-L. A posteriori boundary element error estimation. *Journal of Computational and Applied Mathematics* 1999; **106**:1–19.
15. Paulino GH, Mukherjee S, Ramesh P. Nodal sensitivities as error estimates in computational mechanics. *Acta Mechanica* 1997; **121**:191–213.
16. Shi F, Ramesh P, Mukherjee S. Adaptive mesh refinement of the boundary element method for potential problems by using mesh sensitivities as error indicators. *Computational Mechanics* 1995; **16**(6):379–395.
17. Guiggiani M. Sensitivity analysis for boundary element error estimation and mesh refinement. *International Journal for Numerical Methods in Engineering* 1996; **39**:2907–2920.
18. Charafi A, Wrobel LC. A new h-adaptive refinement scheme for the boundary element method using local reanalysis. *Applied Mathematics and Computation* 1997; **82**:239–271.
19. Varfolomeyev IV, Bush M, Petersilge M. Characterization of the computational accuracy in surface crack problems. *International Journal for Numerical Methods in Engineering* 1998; **41**:721–738.
20. Zhan J, Yokoyama M. An adaptive method for the determination of the element degree for acquiring the desired accuracy in 2-D BEM. *Advances in Engineering Software* 1997; **28**:259–265.
21. Karafiat A. On hp- error estimation in the BEM for a three-dimensional Helmholtz exterior problem. *Computer Methods in Applied Mechanics and Engineering* 1997; **150**:199–214.
22. Liapis S. An adaptive boundary element method for the solution of potential flow problems. *Engineering Analysis with Boundary Elements* 1996; **18**:29–37.
23. Chao R-M, Lee SY. An h-adaptive refinement BEM procedure using modified sample point error analysis in two-dimensional elastic problems. *Advances in Engineering Software* 1999; **30**:227–242.
24. Zhao Z. A simple error indicator for adaptive boundary element method. *Computers and Structures* 1998; **68**:433–443.
25. Ammons BA, Vable M. An hr-method of mesh refinement for boundary element method. *International Journal for Numerical Methods in Engineering* 1998; **43**:979–996.
26. Huebner KH, Thornton EA, Byrom TG. *Finite Element Method for Engineers* (3rd edn). Wiley-Interscience: New York, 1995.
27. Zienkiewicz OC, Taylor RL. The finite element method (4th ed). vol 1. *Basic Formulation and Linear Problems.* McGraw-Hill: New York, 1989.
28. Ainsworth MA, Oden JT. A posteriori error estimation in finite element analysis. *Computer Methods in Applied Mechanics and Engineering* 1997; **142**:1–88.
29. Sun W, Zamani NG. An adaptive h-r boundary element algorithm for the Laplace equation. *International Journal for Numerical Methods in Engineering* 1992; **33**:537–552.
30. Zamani NG, Sun W. Adaptive r and h-r algorithms for boundary elements. *Advances in Engineering Software* 1992; **15**:241–247.
31. Kita E, Higuchi K, Kamiya N. r- and hr-adaptive boundary element method for two-dimensional potential problem. *Computers and Structures* 2000; **74**(1):11–19.
32. Paris F, Cañas J. *Boundary Element Method—Fundamentals and Applications*. Oxford University Press: New York, 1997.
33. Press WH, Teukolsky SA, Vetterling WT, Flannery BP. *Numerical recipes in FORTRAN—The Art of Scientific Computing* (2nd edn). Cambridge University Press: Cambridge, 1992.
34. Jaswon MA, Symm GT. *Integral Equation Methods in Potential Theory and Elastostatics*. Academic Press: London, 1977.
35. Jorge AB, Ribeiro GO, Cruse TA, Fisher TS. Self-Regular Boundary Integral Equation Formulations for Laplace's Equation in 2-D. *International Journal for Numerical Methods in Engineering* 2001; **51**:1–29.
36. Nash SG, Sofer A. *Linear and Non-linear Programming*. McGraw-Hill: New York, 1996.

